

# Homogeneous ice nucleation rates for mW and TIP4P/ICE models through Lattice Mold calculations <sup>EP</sup>

Cite as: J. Chem. Phys. **157**, 094503 (2022); <https://doi.org/10.1063/5.0101383>

Submitted: 31 May 2022 • Accepted: 19 July 2022 • Accepted Manuscript Online: 19 July 2022 •  
Published Online: 02 September 2022

 Ignacio Sanchez-Burgos,  Andres R. Tejedor,  Carlos Vega, et al.

## COLLECTIONS

Paper published as part of the special topic on [Fluids Meet Solids](#)

 This paper was selected as an Editor's Pick



View Online



Export Citation



CrossMark

## ARTICLES YOU MAY BE INTERESTED IN

[Extended Wertheim theory predicts the anomalous chain length distributions of divalent patchy particles under extreme confinement](#)

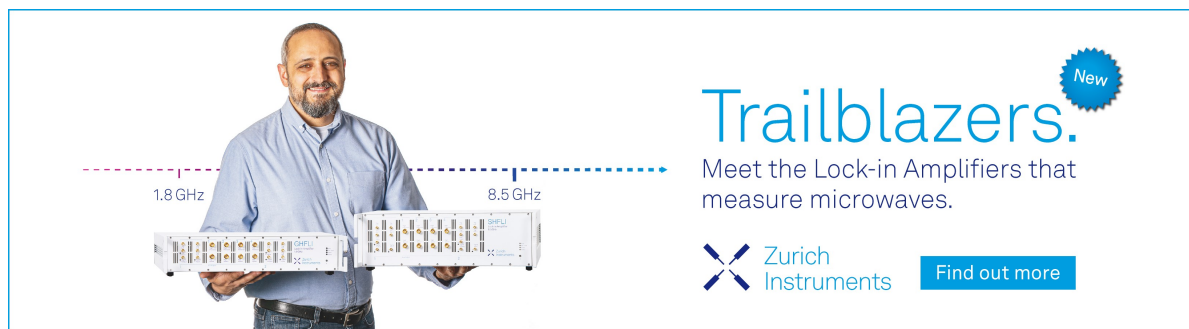
The Journal of Chemical Physics (2022); <https://doi.org/10.1063/5.0098882>

[Nonadiabatic molecular dynamics simulations based on time-dependent density functional tight-binding method](#)

The Journal of Chemical Physics **157**, 084114 (2022); <https://doi.org/10.1063/5.0100339>

[Flow-induced scission of wormlike micelles in nonionic surfactant solutions under shear flow](#)

The Journal of Chemical Physics **157**, 084903 (2022); <https://doi.org/10.1063/5.0096830>



**Trailblazers.** <sup>New</sup>

Meet the Lock-in Amplifiers that measure microwaves.

Zurich Instruments [Find out more](#)

# Homogeneous ice nucleation rates for mW and TIP4P/ICE models through Lattice Mold calculations

Cite as: J. Chem. Phys. 157, 094503 (2022); doi: 10.1063/5.0101383

Submitted: 31 May 2022 • Accepted: 19 July 2022 •

Published Online: 2 September 2022



View Online



Export Citation



CrossMark

Ignacio Sanchez-Burgos,<sup>1</sup>  Andres R. Tejedor,<sup>2</sup>  Carlos Vega,<sup>3</sup>  Maria M. Conde,<sup>2</sup>  Eduardo Sanz,<sup>3,a)</sup>   
Jorge Ramirez,<sup>2,a)</sup>  and Jorge R. Espinosa<sup>1,a)</sup> 

## AFFILIATIONS

<sup>1</sup> Cavendish Laboratory, Department of Physics, Maxwell Centre, University of Cambridge, J J Thomson Avenue, Cambridge CB3 0HE, United Kingdom

<sup>2</sup> Department of Chemical Engineering, Universidad Politécnica de Madrid, José Gutiérrez Abascal 2, 28006 Madrid, Spain

<sup>3</sup> Departamento de Química Física, Facultad de Ciencias Químicas, Universidad Complutense de Madrid, 28040 Madrid, Spain

**Note:** This paper is part of the JCP Special Topic on Fluids Meets Solids.

**a) Authors to whom correspondence should be addressed:** [esa01@ucm.es](mailto:esa01@ucm.es); [jorge.ramirez@upm.es](mailto:jorge.ramirez@upm.es); and [jr752@cam.ac.uk](mailto:jr752@cam.ac.uk)

## ABSTRACT

Freezing of water is the most common liquid-to-crystal phase transition on Earth; however, despite its critical implications on climate change and cryopreservation among other disciplines, its characterization through experimental and computational techniques remains elusive. In this work, we make use of computer simulations to measure the nucleation rate ( $J$ ) of water at normal pressure under different supercooling conditions, ranging from 215 to 240 K. We employ two different water models: mW, a coarse-grained potential for water, and TIP4P/ICE, an atomistic nonpolarizable water model that provides one of the most accurate representations of the different ice phases. To evaluate  $J$ , we apply the Lattice Mold technique, a computational method based on the use of molds to induce the nucleus formation from the metastable liquid under conditions at which observing spontaneous nucleation would be unfeasible. With this method, we obtain estimates of the nucleation rate for ice Ih and Ic and a stacking mixture of ice Ih/Ic, reaching consensus with most of the previously reported rates, although differing with some others. Furthermore, we confirm that the predicted nucleation rates obtained by the TIP4P/ICE model are in better agreement with experimental data than those obtained through the mW potential. Taken together, our study provides a reliable methodology to measure nucleation rates in a simple and computationally efficient manner that contributes to benchmarking the freezing behavior of two popular water models.

Published under an exclusive license by AIP Publishing. <https://doi.org/10.1063/5.0101383>

## I. INTRODUCTION

When liquid water is supercooled below its melting temperature, freezing occurs through a two-step mechanism: the first step being the emergence of an ice embryo and the second its subsequent growth driving crystallization of the whole system. Generally, impurities in water assist the formation of a solid nucleus that, once it reaches a certain critical size, promotes irreversible crystal growth.<sup>1–3</sup> However, in the absence of impurities, the liquid phase can remain metastable for a certain amount of time (depending on the supercooling conditions and the sample size) before undergoing the liquid-to-crystal transition. This phenomenon is termed

homogeneous nucleation, and it is an activated process in which the system must overcome a free energy barrier to form the critical cluster.<sup>4–6</sup>

Understanding ice formation is extremely relevant in different fields such as atmospheric science,<sup>7–12</sup> food industry,<sup>13,14</sup> physics,<sup>5,15–17</sup> and geology.<sup>18,19</sup> One magnitude which is important to understand and characterize is the nucleation rate, which accounts for the typical time that it will take the system at some given conditions to form the critical nucleus. More technically, the nucleation rate ( $J$ ) is defined as the number of critical clusters formed per unit of volume and time. Experiments on homogeneous ice nucleation are typically performed with micrometer-sized water droplets

at temperatures ranging between 230 and 242 K.<sup>17,20–26</sup> Below this range, water freezes instantaneously (within timescales of the order of milliseconds or less), while at higher temperatures, freezing requires inaccessibly long timescales.<sup>27</sup> However, some experiments with nanosized water droplets have been able to measure nucleation rates in the so-called “no-man’s land,” which represents an extremely low temperature range from 200 to 230 K.<sup>28–31</sup>

Computer simulations have proved to be useful in evaluating nucleation rates for many different systems, ranging from Hard Spheres,<sup>32–37</sup> Lennard-Jones,<sup>34,38–45</sup> NaCl,<sup>46–49</sup> and different ionic salts,<sup>50,51</sup> among many other systems.<sup>52–55</sup> Specifically, and due to its aforementioned importance, ice nucleation has been extensively studied by means of computer simulations.<sup>27,34,56–61</sup> Previous efforts have made use of different computational methods, such as Forward Flux Sampling (FFS),<sup>62</sup> Transition Path Sampling (TPS),<sup>63</sup> Metadynamics,<sup>64,65</sup> Umbrella Sampling (US),<sup>66</sup> and Seeding.<sup>27</sup> Some of them are exact (FFS and TPS) or almost exact (US and Metadynamics) and provide rigorous values of  $J$ . Although these techniques use an order parameter as reaction coordinate to follow or drive the liquid-to-solid transition,<sup>33,58,64,65,67</sup> their values of  $J$  do not depend, in practice, on the choice of the order parameter. However, they are computationally very expensive.<sup>49,68–70</sup> In contrast, we have recently proposed another technique denoted as Seeding, which is computationally very efficient and relies on the Classical Nucleation Theory (CNT).<sup>34,35,44,52,71–75</sup> This technique provides reliable results of  $J$  provided that the order parameter is chosen with care. However, admittedly, the results of Seeding depend on the choice of the order parameter,<sup>76</sup> which is in contrast with the rigorous techniques described above.

In this work, we employ the Lattice Mold (LM) technique<sup>77</sup> to compute homogeneous ice nucleation rates. By evaluating the required free energy of creating a precritical cluster, and the rate of such cluster to induce crystallization,  $J$  can be estimated in a computationally efficient manner that does not rely on any theory (i.e., CNT) or choice of the local order parameter (in contrast with the Seeding technique). Nevertheless, although in LM, no traditional order parameters are used, the reaction coordinate to drive crystallization consists of a mold of potential wells (where the crystal density and lattice mold positions assume a given structure) that promotes the formation of a precritical cluster. Admittedly, LM is more expensive than Seeding, but it is still computationally efficient. Previously, LM has been successfully validated for the calculation of nucleation rates of Hard Spheres and the Tosi–Fumi NaCl model,<sup>77</sup> and here, it is adopted to measure ice nucleation rates within a temperature range that includes both micrometer- and nanometer-sized water droplet experiments.<sup>17,20–22,24–26,28,29,31</sup> We first apply the LM technique to the case of ice nucleation in the monoatomic water (mW) model,<sup>78</sup> a coarse-grained description of water that mimics the hydrogen-bonding structure of water by means of a nonbonded angular dependent term that encourages tetrahedral configurations. Once we compare and validate the rates for the mW potential, we extend this technique to the TIP4P/ICE<sup>79</sup> model, which describes water atomistically as a nonpolarizable rigid molecule. The TIP4P/ICE model provides outstanding predictions of the solid and supercooled liquid properties of water, including the phase diagram, equations of state, ice growth rate, and interfacial free energy for the ice Ih–water interface,<sup>61,79,80</sup> which is remarkable considering the anomalous behavior of supercooled water.<sup>81–83</sup> We

apply the LM technique to shed light on the nucleation rate of the TIP4P/ICE model at 230 K and normal pressure, which is currently under debate.<sup>60,68,84</sup> Overall, with our calculations, we aim to find a consensus on the ice nucleation rates of these two popular water models by means of a novel and computationally efficient rare event method.

## II. METHODOLOGY

### A. The Lattice Mold technique

Lattice Mold is a computational approach that can provide reliable estimations of the nucleation rate as previously shown for hard spheres and molten NaCl.<sup>77</sup> Within the LM framework, nucleation is induced by introducing a mold of potential energy wells with the crystal lattice of a given solid phase within the metastable liquid, as illustrated in Fig. 1(a)—similar in methodology to the Mold Integration technique for the calculation of coexistence liquid–solid interfacial free energies.<sup>35,85,86</sup> The interactions between the particles of the system (water) and the “virtual particles” of the mold is described by a square-well (SW) potential (a continuous version of it to obtain forces analytically) that induces the ordering of water molecules into a solid structure (ice in this case). The technique consists of two distinct steps: First, the reversible work to form a precritical cluster is computed by gradually switching on the interaction between the mold and the liquid molecules. Second, independent simulations are conducted to measure the average required time for the induced precritical cluster to complete crystallization (i.e., overcome the remaining nucleation free energy barrier). Initially, the free energy difference between the liquid and the liquid with such precritical cluster is

$$\Delta G^* = \epsilon_m N_w - \int_0^{\epsilon_m} d\epsilon_{SW} \langle N(\epsilon_{SW}) \rangle, \quad (1)$$

where  $\epsilon_m$  is the maximum well depth to evaluate this integral, which ensures that all the sites in the mold will be occupied,  $\langle N(\epsilon_{SW}) \rangle$  is the average number of mold sites occupied by liquid molecules at a given  $\epsilon_{SW}$  value, and  $N_w$  is the total number of wells. This integral is evaluated numerically by performing several Molecular Dynamics (MD) simulations at different well depths ( $\epsilon_{SW}$ ). We compute the average number of occupied sites by dividing the potential energy of the water–well interaction by the well depth ( $\epsilon_{SW}$ ). It is crucial to make sure that the integral is reversible so that the cluster induced by the mold cannot be sustained in the absence of potential wells and quickly dissolves once the interaction between the mold and the liquid molecules is switched off. Since in LM simulations the position and orientation of the mold are imposed, this constraint must also be reflected in the calculation of the free energy such that

$$\Delta G/(k_B T) = \Delta G^*/(k_B T) + \ln(\rho_f V_w) - \ln(8\pi^2), \quad (2)$$

where  $k_B$  is the Boltzmann constant,  $T$  is the temperature,  $\rho_f$  is the fluid number density, and  $V_w$  is the volume of a well. The second and third terms on the right-hand side of Eq. (2) account for the translational and orientational corrections to the free energy for imposing a fixed position and orientation to the induced cluster,

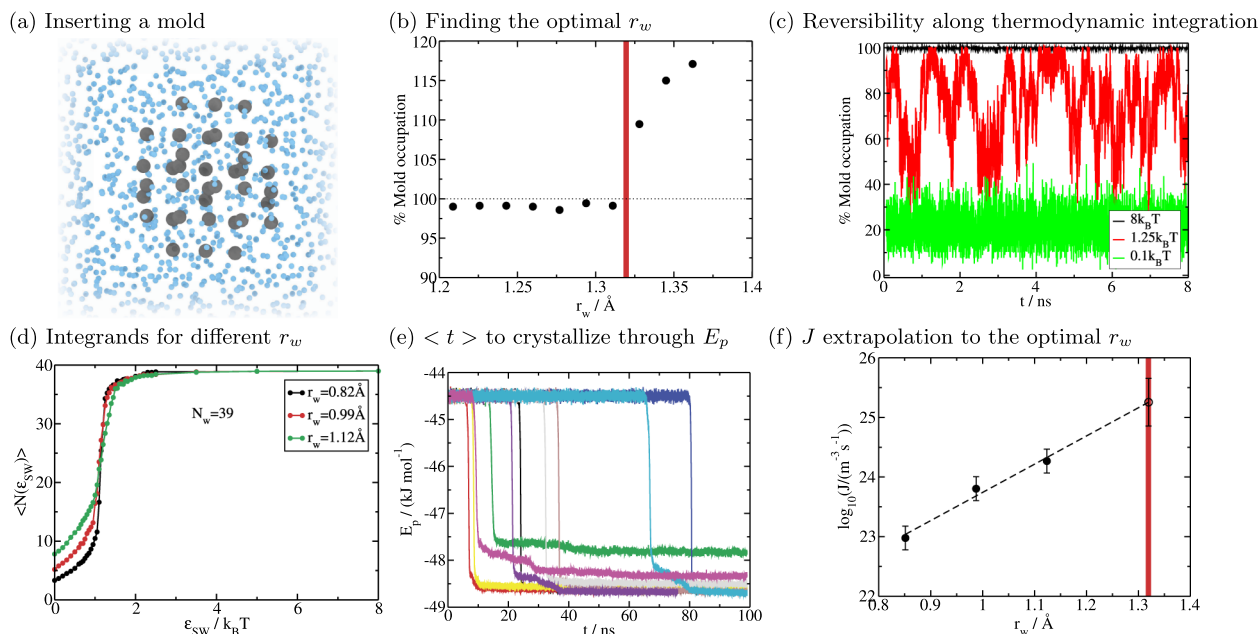


**FIG. 1.** Illustrating the LM technique through the mW water model at  $T = 220$  K and  $p = 1$  bar. (a) Snapshot of a spherical mold of 39 wells (depicted by gray spheres) inserted in water (light blue particles). This and the following snapshots were rendered using OVITO.<sup>95</sup> (b) Average mold occupancy (composed of a single well) as a function of the well width  $r_w$  in a liquid simulation equilibrated at 220 K and 1 bar, with a value of  $\epsilon_{SW} = 8k_B T$ , the minimum required energy for ensuring full occupancy of the potential wells at any time. The horizontal dotted line indicates the limit at which one well is occupied by a single water molecule while the vertical red line depicts the chosen optimal value of  $r_w$ , for the extrapolation of the nucleation rate—threshold value at which the average occupancy becomes greater than one. (c) Percentage of occupied potential wells within the mold shown in Panel (a) for a given  $r_w$  (1.12 Å) using different  $\epsilon_{SW}$  values as indicated in the legend. (d) Average number of occupied wells as a function of the well depth  $\epsilon_{SW}$  for distinct  $r_w$  values (as indicated in the legend). The different curves correspond to the integrand of Eq. (1). (e) Potential energy time-evolution of ten independent trajectories at  $\epsilon_{SW} = 8k_B T$  to compute  $\langle t \rangle$ . The rapid decay in the potential energy corresponds to the time at which water irreversibly freezes.<sup>96</sup> (f) Decimal logarithm of the nucleation rate obtained for different well widths and extrapolation to the optimal  $r_w$  (represented by an empty circle). The red line depicts the optimal width of  $r_w = 1.32$  Å determined in Panel (b).

respectively. The probability per unit volume of finding a crystal cluster of the size of the one induced by the mold ( $P$ ) is given by

$$P = \rho_f \exp(-\Delta G/(k_B T)). \quad (3)$$

For the second step, we carry out independent simulations with the precritical cluster sustained by the mold and calculate the induction time of nucleation. This second step of the technique gives an average induction time  $\langle t \rangle$ , which in combination with the first step provides an estimation of the nucleation rate ( $J$ ),

$$J = P/\langle t \rangle. \quad (4)$$

It is crucial that the cluster formed by the wells is precritical so that the integral of Eq. (1) can be evaluated reversibly (i.e., not inducing crystallization of the system along the integration pathway). This is initially checked by performing simulations with different mold sizes (i.e., different number of wells) at  $\epsilon_m$ . Then, we choose the smallest mold that results in complete crystallization after an induction time that is computationally affordable. By applying this protocol, we guarantee: (i) reversibility in Eq. (1); and (ii) minimization of the imposed constraint across the transition state. Nevertheless, as long as the chosen mold presents induction time

before promoting system crystallization, the choice of the mold size does not alter the obtained nucleation rate, as discussed in Ref. 77. Taken together, the two steps of this technique provide the free energy of forming a precritical cluster and the time required for such a cluster to overcome the nucleation free energy barrier.

## B. Simulation details

In this work, we employ the mW<sup>78</sup> and TIP4P/ICE<sup>79</sup> water models to study homogeneous ice nucleation at normal pressure. Intermolecular potential details can be found in the respective model references. Simulations were performed with the Large-scale Atomic/Molecular Massively Parallel Simulator (LAMMPS) Molecular Dynamics package<sup>87</sup> in the NVT ensemble (with  $N$  equal to the number of particles,  $V$  the volume, and  $T$  the temperature), keeping  $T$  constant with the Nosé–Hoover thermostat.<sup>88–90</sup> Additionally, we compute equations of state in order to obtain mold structures with a relaxed density by performing NpT simulations, fixing the pressure ( $p$ ) with the Nosé–Hoover barostat.<sup>88–90</sup> We integrate the equations of motion using the velocity-Verlet integrator. The simulation time step chosen is 3 fs for the mW model and 2 fs for the TIP4P/ICE model, and the thermostat relaxation time is 0.1 ps for the mW potential and 2 ps for the TIP4P/ICE model. In NpT simulations,

the barostat relaxation time is 0.5 and 2 ps for mW and TIP4P/ICE models, respectively.

For consistency with previous nucleation rate calculations of both models,<sup>15,34,56,57,59–61,68,91</sup> we set the potential cutoff at 8.5 and 4.3 Å for TIP4P/ICE and mW, respectively. Moreover, for the TIP4P/ICE model, long-range Coulombic interactions are treated with the *pppm/tip4p* particle–particle particle–mesh (PPPM) solver in LAMMPS<sup>92</sup> with a relative error in forces of  $10^{-5}$ . Long-range corrections to the Lennard-Jones part of the potential for energy and pressure are also applied. While in the mW model the potential cutoff (4.3 Å) is an intrinsic model parameter that cannot be modified, we check that for the TIP4P/ICE model, the neglected potential energy contribution of employing a short cutoff (8.5 Å instead of a long cutoff such as 15 Å) is lower than 0.05% when evaluating the potential energy of a bulk liquid phase applying PPPM and long-range corrections (for further insights on potential truncation effects on ice nucleation, please see Ref. 93). Finally, for the TIP4P/ICE model, we keep the O–H bond length and H–O–H angle values constant with the Shake algorithm implemented in LAMMPS.<sup>94</sup>

To implement the LM technique, we simulate the potential wells' interaction with water molecules using a square-well like (i.e., continuous) potential (SW)<sup>86</sup> of the following form:

$$u_{SW} = -\frac{1}{2}\epsilon_{SW}\left[1 - \tanh\left(\frac{r - r_w}{\alpha}\right)\right], \quad (5)$$

where  $\epsilon_{SW}$  is the depth of the potential energy well,  $r_w$  is the radius of the attractive well,  $\alpha$  controls the steepness of the well, and  $r$  is the distance between water molecules and the center of the wells. We choose  $\alpha = 0.017$  Å as discussed in Ref. 86. In practice, for the TIP4P/ICE model, this is the effective interaction between oxygen atoms and the wells, while hydrogen atoms have no interaction with the wells and spontaneously arrange into the correct orientation of the lattice. It is interesting to point out that the wells' positions are fixed (i.e., they act as an external field) and we only integrate the positions of water. LM simulations are performed in the NVT canonical ensemble (to keep fixed the crystal lattice positions of the mold along the calculation), and the density of the system is chosen as that of a bulk liquid at the temperature and pressure (1 bar in this work) of interest. We make the simulation box large enough so that the emergence of the precritical nucleus barely alters the desired pressure. We also note that although in this work we compute nucleation rates at different temperatures along a given isobar (1 bar), the LM technique can be indistinctly applied to evaluate pressure-dependent rates (i.e., across an isotherm) as long as the metastable liquid and the crystal mold display their characteristic equilibrium density of the state of interest ( $p$ ,  $T$ ).

### III. RESULTS

#### A. Work example: Computing the nucleation rate of mW water through the Lattice Mold technique

We first focus on the crystal nucleation of mW at 220 K and 1 bar by means of the LM technique. As discussed in Ref. 77, the use of molds consisting of potential wells of a limited width constrains the solid structure, hence, leading to a moderate overestimation of the free energy barrier ( $\Delta G$ ). Such an effect can be minimized by calculating  $\Delta G$  with wells that are in the limit of fitting two

water molecules at the same time, to avoid constraining the crystal lattice and providing correct estimates of the nucleation rate. To find the optimal well width that does not constrain the induced nuclei, we perform simulations of the liquid phase with one well of  $\epsilon_{SW} = 8k_B T$  (sufficient well depth to completely fill the well) and we measure the average occupation of such a well with different potential widths. Reaching the maximum well radius before the occurrence of double-particle occupation ensures negligible translational constraint of confining a water molecule within a given position in the mold crystal lattice. In Fig. 1(b), we plot the average occupation of a well inserted into an equilibrated liquid at 220 K and 1 bar as a function of  $r_w$ . We find that the optimal width is 1.32 Å, the limit at which the average occupation of a single well is roughly 100%.

Since it would be incorrect to evaluate the nucleation rate by Eq. (4) with a mold of potential wells in the limit of double-particle occupancy, we measure the nucleation rate at different well widths lower than the optimal one, and we later proceed to extrapolate to 1.32 Å. We choose to apply the LM technique at  $r_w$  values of 0.85, 0.99, and 1.12 Å and solve Eq. (1) by performing several simulations at different  $\epsilon_{SW}$ . To achieve this, we run simulations of a liquid with a mold of potential wells forming a spherical cluster with the equilibrium positions of the stable crystal phase at such conditions (ice Ih). The integrand of Eq. (1) is the average number of occupied wells ( $\langle N(\epsilon_{SW}) \rangle$ ) at different values of  $\epsilon_{SW}$ . In Fig. 1(c), we show the time-evolution of the mold average occupancy for three different simulations exhibiting low, middle, and high mold occupancy, at values of  $\epsilon_{SW}$  of 0.1, 1.25, and  $8k_B T$ , using a potential well width of  $r_w = 1.12$  Å. By evaluating the average number of wells as a function of  $\epsilon_{SW}$ , we construct the curves shown in Fig. 1(d) and find the area below the curves, which provides  $\Delta G^*$  through Eq. (1). We have checked that changing the grid intervals of  $\epsilon_{SW}$  from 0.1 to  $0.25k_B T$  along the steepest part of the integrand [i.e., from  $\epsilon_{SW} = 1$  to  $2k_B T$  in Fig. 1(d)] does not result in significant differences in  $\Delta G^*$  (e.g.,  $\sim 0.3k_B T$ ). Nevertheless, it is always recommendable to employ a thin grid in the transition region between mostly empty molds ( $\epsilon_{SW} < 1k_B T$ ) and practically full ones ( $\epsilon_{SW} > 2k_B T$ ) to ensure that such region does not add uncertainty to the computed free energy barriers. Next, we employ Eq. (2) to obtain the free energy of forming a precritical cluster with freedom to translate and rotate. As it can be seen in Fig. 1(c), intermediate  $\epsilon_{SW}$  values along the integrand [Fig. 1(d)] can result in strong fluctuations of the mold occupancy  $N(\epsilon_{SW})$  over time, clearly denoting reversibility along the integration pathway.

Finally, to obtain the nucleation rate we must also compute the rate of the formed precritical cluster to overcome the nucleation free energy barrier and induce crystallization across the whole system. We conduct simulations with the wells enabled at maximum depth,  $\epsilon_m = 8k_B T$ , and find the average time  $\langle t \rangle$  it takes for the cluster to irreversibly grow. In Fig. 1(e), we show the potential energy (just water–water interactions) evolution of ten different trajectories (with different initial velocities) for  $r_w = 1.12$  Å. The dramatic drop in potential energy marks the transformation of the liquid into a solid, therefore, indicating the time required for irreversible growth of a given trajectory.<sup>96</sup> In Table 1, we provide the obtained values of  $\Delta G$  and  $\langle t \rangle$  for the studied well widths ( $r_w$ ). We acknowledge that cluster size and irreversible growth can be tracked by other means, taking for example a local order parameter such as the  $\bar{q}_4 - \bar{q}_6$

**TABLE I.** LM data for the calculation of  $J$  using the mW model at  $T = 220$  K and  $p = 1$  bar: Well widths ( $r_w$ ) at which LM calculations were performed,  $\Delta G$  from Eq. (2), average time to overcome the nucleation free energy barrier ( $t$ ), and logarithm of the nucleation rate, with  $J$  in units of  $m^{-3} s^{-1}$ . The final nucleation rate obtained by extrapolation to the optimal well radius is depicted in boldface font.

mW at 220 K and 1 bar			
$r_w$ (Å)	$\Delta G/k_B T$	$\langle t \rangle$ (ns)	$\log_{10} J$
0.85	31.21	9.8	23.0
0.99	28.80	16.2	23.8
1.12	27.38	29.1	24.2
<b>1.32</b>	<b>Extrapolation to optimal <math>r_w</math></b>		<b>25.3(2.5)</b>

proposed by Lechner and Dellago.<sup>97</sup> However, it is not strictly necessary to monitor the system evolution through a local order parameter as we demonstrate in Fig. 1(e) (using a global indicator as the system potential energy). Please note that when the potential energy reaches values that indicate irreversible growth [i.e.,  $-45$  kJ mol<sup>-1</sup> in Fig. 1(e)], the pressure has only increased 30 bars with respect to the initial pressure ( $p = 1$  bar), negligibly affecting our nucleation rate calculations,<sup>98</sup> hence making the NVT ensemble suitable for the LM technique as long as the total system size is reasonably large (see Table II). Once that average time has been obtained, we can compute the nucleation rate by means of Eq. (4). Finally, in Fig. 1(f), we show the nucleation rate for the three different well widths studied and the extrapolation to the optimal width (see also Table I).

**TABLE II.** Results of the Lattice Mold technique for both mW and TIP4P/ICE water models at  $p = 1$  bar. For each state, crystal structure, temperature ( $T$ ), number of wells in the mold ( $N_w$ ), total number of water molecules in the system ( $N$ ), density of the liquid ( $\rho_{liq}$ ) and solid ( $\rho_{sol}$ ) phases, and nucleation rate logarithm ( $\log_{10} J$ , with  $J$  in units of  $m^{-3} s^{-1}$ ) are provided.

Mold structure	$T$ (K)	$N_w$	$N$	$\rho_{liq}$ (g cm <sup>-3</sup> )	$\rho_{sol}$ (g cm <sup>-3</sup> )	$\log_{10} J$
mW model						
Ice Ih	215	27	10 500	0.9943	0.9838	28.5(2.5)
Ice Ih	220	39	7 460	0.9974	0.9833	25.3(2.5)
Ice Ih	225	57	10 439	0.9998	0.9830	21.0(2.5)
Ice Ih	230	73	10 433	1.0013	0.9826	17.2(2.5)
Ice Ih	235	140	10 401	1.0025	0.9822	6.7(2.5)
Ice Ih	240	214	10 347	1.0030	0.9817	-4.9(2.5)
Ice Ic	235	167	10 121	1.0025	0.9823	6.3(2.5)
Ice Ic	240	256	10 080	1.0030	0.9813	-3.0(2.5)
Ice Ic/Ih Stacking mixture	240	268	9 148	1.0030	0.9815	-5.3(2.5)
TIP4P/ICE model						
Ice Ih	230	214	6 347	0.9417	0.9112	14.1(3.0)

## B. mW nucleation rates

We now apply the LM technique at different temperatures to obtain a broad picture of the mW nucleation scenario at normal pressure (1 bar). We achieve this by inserting spherical molds with an ice Ih lattice that can induce precritical clusters from a temperature range between 215 and 240 K. The inserted molds are spherical and display a perfect ice lattice with the equilibrium density of the bulk crystal structure at each temperature, which was obtained by performing independent NpT simulations of bulk ice. Additionally, we also prepare molds of ice Ic and a stacking mixture of ice Ic/Ih as shown in Fig. 2(a) and Table II. Since ice Ic and Ih share the basal plane [(111) in ice Ic and (0001) in ice Ih], the Ic/Ih mixture was generated by alternating AB layers from ice Ih and ABC from ice Ic stacked along the basal plane, generating a hybrid crystal structure. All mold sizes, number of water molecules in each system, solid and liquid densities, and nucleation rates for the different states are reported in Table II. In Fig. 2(a), we show snapshots of a typical simulation box for the LM technique, along with closer views of three different molds employed at  $T = 240$  K (pure Ih, pure Ic, and Ih/Ic stacking mixture) surrounded by water molecules. In Fig. 2(b), we plot the nucleation rate obtained by using LM for the three different structures compared with previous results obtained through different rare event techniques and brute force simulations.<sup>15,34,56,58,59,91</sup>

We find good agreement with the results obtained by Li *et al.*<sup>56</sup> by means of Forward Flux Sampling and by both Russo *et al.*<sup>58</sup> and Cheng *et al.*<sup>59</sup> through Umbrella Sampling simulations. In contrast, some disagreement is found with the nucleation rates obtained by Haji-Akbari *et al.* using Forward Flux Sampling calculations at 230 and 235 K.<sup>57</sup> Nevertheless, those calculations were recently revisited in Ref. 91 by the same author providing nucleation rates in excellent agreement with Refs. 56, 58, and 59 as well as with our present calculations (Fig. 2). The extrapolated trend of our results toward higher supercooling is also consistent with the nucleation rate of Moore and Molinero<sup>15</sup> obtained by means of brute force simulations at low temperatures (200 K). Seeding results obtained by Espinosa *et al.*<sup>34</sup> are 4 orders of magnitude below the ones obtained through LM; however, this discrepancy lies within the uncertainty of Seeding calculations, which is of about 5 orders of magnitude due to the reliance of Seeding simulations on local order parameters to identify the number of particles in the critical cluster.<sup>76</sup> The excellent agreement between the predicted nucleation rates obtained through LM and previous calculations<sup>15,34,56,58,59,91</sup> indirectly evidences that the choice of the mold size barely alters the obtained nucleation rates by this technique as discussed in Ref. 77.

Importantly, when comparing the different ice structures Ic, Ih, and the Ic/Ih stacking mixture, we roughly find the same nucleation rate for all structures within the uncertainty at the distinct studied temperatures: between pure ice Ic and Ih nuclei at 235 K and among pure ice Ic and Ih as well as with an ice Ic/Ih stacking mixture mold at 240 K [see Table II and Fig. 2(b)]. Please note that we only generate a mold of a stacking mixture of Ic/Ih at 240 K so that the mold, and consequently the induced precritical cluster, is large enough to display ice stacking disorder across the basal plane of the two competing crystal structures while maintaining the least possible surface/volume ratio (i.e., spherical shape). A higher fraction of interfacial particles in smaller clusters (i.e., molds of  $\sim 150$  wells at 235 K) would lead to minimal stacking differences between pure ice

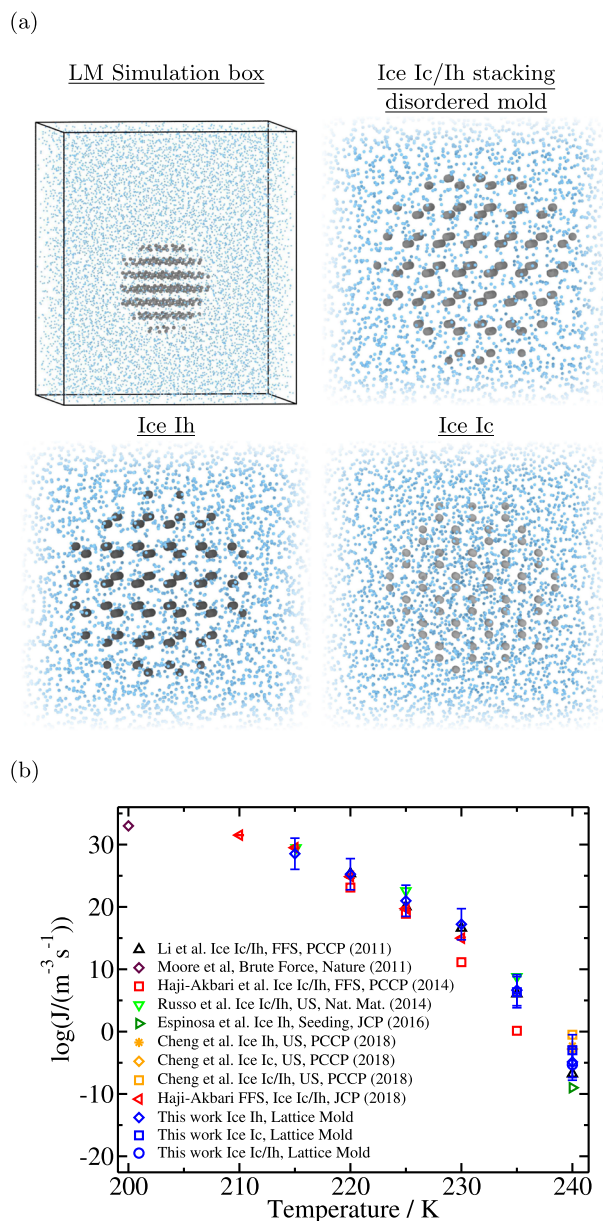


**FIG. 2.** (a) Representative simulation box employed for the LM technique, along with close views of the molds with the three ice lattices used at 240 K. Water molecules are depicted in light blue while the mold wells are colored in gray. (b) Decimal logarithm of the nucleation rate as a function of temperature at normal pressure for the mW model. We include previous calculations<sup>15,34,56,58,59,91</sup> as indicated in the legend and discussed in the text along with those computed through the LM technique. The ice polymorph/s for which the nucleation rate corresponds is provided in the legend.

Ic or Ih molds and stacking mixture molds (with negligible differences at even lower temperatures). Results reported by Cheng *et al.*<sup>59</sup> already suggested that the nucleation rate of ice Ic and Ih are very similar, while that of the Ih/Ic stacking mixture is moderately higher

(i.e., 2 orders of magnitude). In our case, we find that at 240 K and 1 bar, the nucleation rate of a stacking mixture nucleus is within the uncertainty of those of pure ice Ic and Ih. For the rest of previous calculations,<sup>56–58,91</sup> the employed rare event methods were not biasing *a priori* the nucleating ice polymorph; hence, their calculations are ascribed to mixtures of both polymorphs, although ice Ih is usually the dominant phase. Overall, our results in Fig. 2(b), where we compare LM results with other previous calculations for the mW model, reaffirm the validity of this technique, which had previously been proven for Hard Spheres and NaCl Tosi–Fumi models.<sup>77</sup>

### C. TIP4P/ICE nucleation rates

Once the results of  $J$  for the mW potential are computed, we apply the same methodology to evaluate the nucleation rate of the TIP4P/ICE model,<sup>79</sup> an accurate potential for describing supercooled water and the different ice phases.<sup>83,99–102</sup> We carry out our calculations at 230 K and normal pressure, conditions at which the homogeneous nucleation rate has been previously reported, making use of Metadynamics,<sup>60</sup> FFS,<sup>68,91</sup> and Seeding<sup>84</sup> calculations. The reported values of  $J$  obtained by means of these different techniques significantly disagree in several orders of magnitude; with the results obtained by Niu *et al.*<sup>60</sup> being 9 orders of magnitude greater than those of Haji-Akbari and Debenedetti.<sup>68</sup> The revisited work of this calculation by Haji-Akbari<sup>91</sup> did not calculate the nucleation rate directly, but it estimates a value of  $J$  4 orders of magnitude higher than the original published value in Ref. 68, thus reducing the discrepancy to 5 orders of magnitude. Moreover, Seeding results obtained by Espinosa *et al.*<sup>84</sup> were extrapolated towards lower temperatures using CNT-like fits<sup>34</sup> and provided a nucleation rate 5 orders of magnitude greater than those reported by Niu *et al.*<sup>60</sup> Although such differences lie within the uncertainty of both calculations (Metadynamics has  $\sim 2$  orders of magnitude of uncertainty and Seeding  $\sim 5$  orders of magnitude when the mislabeling criterion is used to identify molecules as liquid-like or solid-like<sup>34</sup>), there is a noticeable difference of 10 orders of magnitude between the Seeding results and those of Haji-Akbari<sup>91</sup> (far beyond the uncertainty between both methodologies, with the reported uncertainty of FFS being  $\sim 1$  order of magnitude<sup>91</sup>).

The procedure used within the LM framework for the TIP4P/ICE is identical to that followed for the mW model. By inserting a mold that creates a precritical cluster in the liquid [214 wells, see snapshot in Fig. 3(a)], we are able to perform multiple simulations at different well depths ( $\epsilon_{sw}$ ) ranging from 0 to  $10k_B T$ , and consequently solve Eq. (1). Once we have obtained the free energy of formation of such precritical cluster induced by the mold, we calculate the average time it takes to overcome the nucleation free energy barrier. Gathered this information, we apply Eq. (4) to compute  $J$ . In the same way as we do for the mW model, we compute the nucleation rate at  $r_w$  values of 0.95, 1.02, 1.09, 1.1, and 1.23 Å and extrapolate  $J$  to the optimal well width of 1.36 Å in this case.

A snapshot of the employed mold in TIP4P/ICE LM calculations is shown in Fig. 3(a). A summary of these calculations, providing the number of wells in the mold, nucleation rate, and density of the stable (Ih) and metastable (liquid) phases, can be found in Table II. Moreover, further details on the free energy needed to form a precritical cluster with the employed mold as well as the induction

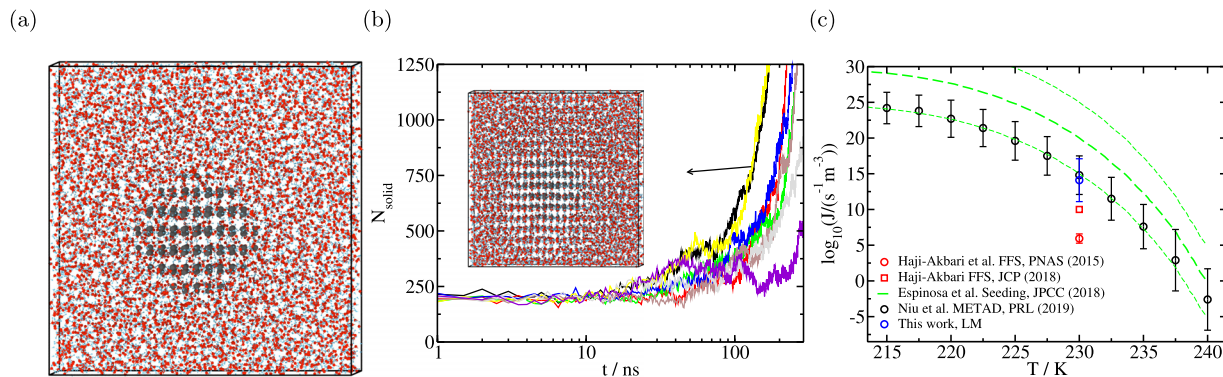


**FIG. 3.** Lattice Mold technique for the nucleation rate calculation of the TIP4P/ICE model. (a) Snapshot of a configuration of liquid water in which a mold of ice Ih with 214 potential wells is inserted at 230 K and 1 bar. Red and blue particles represent the oxygen and hydrogen atoms of water, respectively, while gray particles depict the inserted mold of potential wells. (b) Number of particles in the crystal nucleus ( $N_{\text{solid}}$ ) against time for eight different independent trajectories at  $\epsilon_{\text{SW}} = 10k_B T$  and  $r_w = 1.09 \text{ \AA}$  to compute  $\langle t \rangle$ .  $N_{\text{solid}}$  is determined through the  $\bar{q}_6$  local order parameter<sup>97</sup> as specified in Ref. 61. Inset: Snapshot of a system enclosing a post-critical cluster in the process of growing irreversibly (i.e., containing  $\sim 1000$  molecules). (c) Decimal logarithm of the nucleation rate as a function of temperature for the TIP4P/ICE model at 1 bar. We compare our LM results with those from FFS by Haji-Akbari and Debenedetti<sup>68</sup> (and the revisited work<sup>91</sup>), Seeding results reported by Espinosa *et al.*,<sup>84</sup> and Metadynamics results reported by Niu *et al.*<sup>60</sup> The upper and lower (thin) dashed green lines indicate the Seeding uncertainty in  $J$ .

time to complete nucleation are reported in Table III. Additionally, in Fig. 3(b), we plot the number of water molecules in the crystal nucleus as a function of time for eight different trajectories at a well radius of  $r_w = 1.09 \text{ \AA}$ , through which we obtain  $\langle t \rangle$  [required for Eq. (4)]. The result of the nucleation rate against temperature is shown in Fig. 3(c) along with the results obtained by Niu *et al.* through Metadynamics,<sup>60</sup> by Espinosa *et al.* through Seeding,<sup>84</sup> and by Haji-Akbari and Debenedetti<sup>68</sup> (also including the revisited correction from Ref. 91) via FFS. We find excellent agreement between our results and those of Niu *et al.*<sup>60</sup> We predict a nucleation rate of  $\log_{10}(J/\text{m}^{-3} \text{ s}^{-1}) = 14.1(3.0)$ , which matches within the uncertainty of the Metadynamics logarithm of the nucleation rate of 14.8(2.7) reported by Niu *et al.*<sup>60</sup> Seeding results are 5 orders of magnitude apart, which is a reasonable agreement given the nature of the Seeding technique and the fact that 230 K is an extrapolated state

**TABLE III.** LM data for the calculation of  $J$  using the TIP4P/ICE model at 230 K and 1 bar: Well widths ( $r_w$ ) at which LM calculations were performed,  $\Delta G$  from Eq. (2), average time to overcome the nucleation free energy barrier  $\langle t \rangle$ , and logarithm of the nucleation rate, with  $J$  in units of  $\text{m}^{-3} \text{ s}^{-1}$ . The final nucleation rate obtained by extrapolation to the optimal well radius is shown in boldface font.

TIP4P/ICE at 230 K and 1 bar			
$r_w$ ( $\text{\AA}$ )	$\Delta G/k_B T$	$\langle t \rangle$ (ns)	$\log_{10} J$
0.95	57.85	92	10.4
1.02	55.57	118	11.3
1.09	53.71	128	12.1
1.16	52.33	136	12.6
1.23	51.33	273	12.8
<b>1.36</b>	<b>Extrapolation to optimal <math>r_w</math></b>		<b>14.1(3.0)</b>

from direct Seeding measurements at lower supercooling.<sup>34,84</sup> Additionally, we find a moderate disagreement with the revisited FFS calculation by Haji-Akbari,<sup>91</sup> which lies 5 orders of magnitude lower than our LM calculations and the recently reported nucleation rates using Metadynamics simulations.<sup>60</sup>

Remarkably, we note that much larger discrepancies between nucleation rates from different authors can be found for the TIP4P/ICE model [Fig. 3(c)] than for the mW potential [Fig. 2(b)]. We hypothesize that the reason behind such fact is the much better sampling (due to a faster relaxation time) that can be attained with the mW potential compared to the atomistic TIP4P/ICE model.<sup>61</sup> Generally, nucleation rate discrepancies among different rare event techniques have emerged at low supercooling states where extremely large sampling is required.<sup>91</sup> For instance, in FFS calculations, inconsistencies have emerged when a notorious number of milestones needs to be employed to connect the metastable state with the critical cluster. That usually happens at low metastabilities, and it is especially accentuated in computationally expensive models with long relaxation times such as the TIP4P/ICE model here compared to the mW potential.<sup>68</sup> That FFS is more prone to underestimate  $J$  at low supercooling is supported by the nucleation rates computed via FFS at 230 and 235 K from Ref. 57 [shown in Fig. 2(b)] where inconsistent values compared to the rest of techniques were reported only at moderate supercooling (i.e., 230 and 235 K at 1 bar), while at deep supercooling (i.e., from 215 to 225 K at 1 bar), good agreement with different independent calculations was found. Moreover, it has been recently noted in oppositely charged colloids that such lack of extreme sampling under conditions of low metastability may lead to underestimated values of  $J$  via FFS calculations.<sup>103</sup> Hence, the better agreement between independent techniques in mW calculations compared to TIP4P/ICE nucleation rates might be due to the less demanding computational effort required to sample the pathway connecting the metastable fluid and the critical cluster in the mW model.<sup>91</sup>

## IV. DISCUSSION AND CONCLUSIONS

A comparison between computational and experimental estimates of the nucleation rate is critical to elucidate how good our understanding of homogeneous ice nucleation is. In Fig. 4, we show the nucleation rate with respect to supercooling conditions ( $\Delta T = T_{\text{melting}} - T$ , where  $T_{\text{melting}}$  is 273 K for the mW model,<sup>104</sup> 270 K for the TIP4P/ICE model,<sup>61</sup> and 273.15 K for real water) for the two studied models against experimental nucleation rates. Experiments performed with microdroplets<sup>17,20–22,24–26</sup> and nano-droplets<sup>28,29,31</sup> are colored in dark and light green, respectively, while results for the mW water model<sup>15,34,56,58,59,91</sup> are colored in blue and those obtained from the TIP4P/ICE model<sup>60,68,84</sup> in red. As depicted in Fig. 4, our understanding of ice nucleation at normal pressure spans over a wide range of temperatures. However, within such range, we can still find discrepancies between different experimental and computational approaches. At supercooling conditions ranging between 30 and 40 K, there is good agreement between all experimental results reported.<sup>17,20–22,24,25</sup> Moreover, estimations of the nucleation rate in the same range for the TIP4P/ICE model also match experimental results, while the mW potential severely underestimates the nucleation rate within  $\sim 10$ – $15$  orders of magnitude. This can be explained by the higher liquid–crystal interfacial free energy of the mW model at that supercooling conditions when compared to the TIP4P/ICE model.<sup>61</sup> However, at greater supercooling conditions (above  $\Delta T = 45$  K), the mW model appears to recover the experimental  $J$  trend.

It is worth noting that, as discussed in Ref. 84, in nano-droplet experiments (depicted by light green symbols in Fig. 4), the pressure inside such drops is larger than the atmospheric one by virtue

of the Laplace pressure, and over  $\Delta T = 50$  K, metastable liquid nano-droplets can reach pressures up to 500 bars. The Seeding curve in Fig. 4 accounts for this effect; however, direct comparison between calculations performed at normal pressure and those of nanoscale experiments can be affected by the higher pressure in the latter, which has a decelerating effect on ice nucleation.<sup>98</sup> Under high supercooling conditions ( $\Delta T > 40$  K), TIP4P/ICE predictions reported by Niu *et al.*<sup>60</sup> moderately underestimate the experimental nucleation rates<sup>17,28,29,31</sup> by 4–6 orders of magnitude. Moreover, in the range  $35 \text{ K} < \Delta T < 50 \text{ K}$ , the mW potential underestimates the experimental nucleation rates by  $\sim 5$ – $10$  orders of magnitude. We hypothesize that the difference in melting enthalpy of both models (and the high value of the ice–liquid interfacial free energy in the case of the mW model) with respect to that of real water might be behind such moderate nucleation rate underestimation (Fig. 4). Whereas the experimental melting enthalpy ( $\Delta H_m$ ) at normal pressure is 1.44 kcal/mol, the same magnitude for both potentials is 1.29 and 1.26 kcal/mol for the TIP4P/ICE and mW models, respectively. Given that the ice–water chemical potential difference ( $\Delta\mu$ ) along an isobar can be approximated until moderate supercooling conditions through  $\Delta\mu = \Delta H_m(1 - T/T_m)$ , where  $T$  indicates temperature and  $T_m$  the melting temperature, we hypothesize that the lower melting enthalpies of both potentials can translate into lower chemical potential differences and, thus, lower driving force to nucleate. Furthermore, it has been suggested that ice nucleation might be favored at the subsurface of water droplets,<sup>106</sup> which would enhance the experimental nucleation rate. Even though there is intense debate in that regard (and still it is not clear whether nucleation may be favored or not; see Refs. 57 and 107), the fact that in computer simulations ice nucleation rates are evaluated in bulk liquid conditions

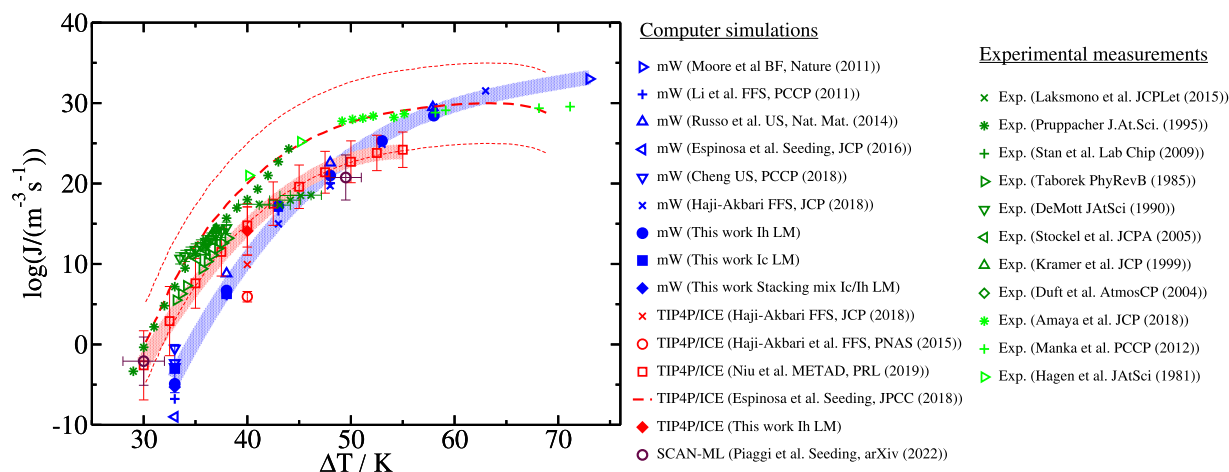


**FIG. 4.** Decimal logarithm of the homogeneous ice nucleation rate against supercooling ( $\Delta T = T_{\text{melting}} - T$ , with  $T_{\text{melting}}$  being 273 K for the mW model,<sup>104</sup> 270 K for the TIP4P/ICE model,<sup>61</sup> and 273.15 K for real water) obtained both through computer simulations (mW and TIP4P/ICE models) and experimental techniques. Microdroplet<sup>17,20–22,24–26</sup> and nano-droplet<sup>28,29,31</sup> experimental rates are colored in dark and light green, respectively,  $J$  values for the mW model<sup>15,34,56,58,59,91</sup> are shown in blue, while TIP4P/ICE results<sup>60,68,84,91</sup> are depicted in red. Red and blue bands depict polynomial fits to TIP4P/ICE and mW nucleation rates, respectively, considering the data from this work and that of Niu *et al.*<sup>60</sup> for the TIP4P/ICE model and  $J$  data obtained from this work and Refs. 15, 56, 58, 59, 61, and 91 for the mW model. Furthermore, nucleation rates through an *ab initio* machine learning model of water by Piaggi *et al.*<sup>105</sup> using Seeding simulations have been included (maroon symbols). Results from this work are represented with filled symbols, while those of other groups are displayed with empty ones. Please note that the Seeding results obtained by Espinosa *et al.*<sup>84</sup> for the TIP4P/ICE model are also represented by a dashed line (including upper and lower bounds for the uncertainty) since the  $J$  value along this regime has been extrapolated from data at lower supercooling using a CNT fit.

(i.e., absence of interfaces) might also explain the lower nucleation rate predictions of both TIP4P/ICE and mW models.

Importantly, the most noticeable disagreement between experiments also occurs within this temperature range where Laksmono *et al.*<sup>26</sup> using microdroplets to measure  $J$  disagree with nanodroplet nucleation rates reported by Manka *et al.*,<sup>29</sup> Hagen *et al.*,<sup>31</sup> and Amaya and Wyslouzil<sup>28</sup> by 8 orders of magnitude. In contrast, TIP4P/ICE Seeding estimations<sup>84</sup> in this regime match the experimental rates reported by Manka *et al.*,<sup>29</sup> Hagen *et al.*,<sup>31</sup> and Amaya and Wyslouzil<sup>28</sup> (although probably due to an overestimation in  $J$  by virtue of the employed local order parameter). The interference of ice growth with ice nucleation in the experiments of Laksmono *et al.*<sup>26</sup> has been hypothesized to be the cause of such discrepancy.<sup>61</sup> Interestingly, we note that under very high supercooling conditions ( $\Delta T > 55$  K), mW nucleation rates become higher than those of TIP4P/ICE (considering that the  $J$  values reported by Niu *et al.* are more accurate than those obtained from Seeding simulations). In fact, spontaneous crystallization of the mW model has been reported by Moore and Molinero<sup>15</sup> near 200 K. The moderately higher  $J$  values of the mW model compared to those of the TIP4P/ICE model at deep supercooling conditions (Fig. 4) on top of the significantly higher crystal growth rate of the mW model ( $\sim 2$  orders of magnitude higher than that of TIP4P/ICE<sup>61</sup>) enables the direct observation of water freezing in mW simulations at large supercooling conditions without the need of rare event techniques. Finally, in Fig. 4, we show the nucleation rate obtained by means of Seeding simulations using SCAN-ML, a recently developed machine learning trained model,<sup>105</sup> which greatly resembles TIP4P/ICE results obtained by Niu *et al.*<sup>60</sup> Remarkably, both TIP4P/ICE and SCAN-ML recover most of the experimental rates within 5–7 orders of magnitude for a wide range of supercooling conditions (Fig. 4).

In summary, here we have computed ice nucleation rates for two popular water models through the Lattice Mold technique, an efficient and simple method that does not rely on any theoretical assumption (i.e., CNT). Our results show good agreement with some previously reported data for both models obtained through FFS,<sup>56</sup> Seeding,<sup>34,84</sup> US,<sup>58,59</sup> and Metadynamics.<sup>60</sup> The computational performance achieved through our method is also of high relevance: More than  $21 \times 10^6$  central processing unit (CPU) hours were required to compute the nucleation rate of the TIP4P/ICE at 230 K via FFS calculations,<sup>68</sup> while through the LM technique, less than  $1 \times 10^6$  of CPU hours were required. Despite the fact that LM calculations are still far more expensive than Seeding simulations—where evaluating the TIP4P/ICE nucleation rate at 230 K costs  $\sim 150\,000$  CPU hours<sup>61</sup>—the technique still has a very good cost balance, especially considering the advantages with respect to Seeding, such as non-reliance on the Classical Nucleation Theory or in regard to the usage of complex local order parameters to determine the critical cluster size.

Overall, multiple publications can provide relatively disparate estimations of the nucleation rate between experiments and simulations for a molecule as essential as water, hence, demonstrating the complexity of these calculations. Despite this, our understanding on the time required to freeze water has considerably improved in the last few decades (Fig. 4), and here we have presented the Lattice Mold technique, aiming to reach consensus on the value of the homogeneous ice nucleation rate for two distinct water models that describe molecular interactions at different levels of resolution.

Establishing a solid and computationally efficient methodology to compute nucleation rates is fundamental, since in the near future, the development and validation of more accurate water models will require feasible and reliable measurements of this critical magnitude controlling atmospheric phenomena and cryopreservation processes.

## ACKNOWLEDGMENTS

This project received funding from the Oppenheimer Research Fellowship of the University of Cambridge. A.R.T. was funded by the Universidad Politécnica de Madrid (Grant No. ESTANCIAS-PIF 20-TYOSR8-13-4N0WPQ) and the Oppenheimer Fellowship. I.S.-B. acknowledges funding from the Derek Brewer scholarship of Emmanuel College and EPSRC Doctoral Training Programme studentship, Grant No. EP/T517847/1. M.M.C. and J.R. acknowledge funding from the Spanish Ministry of Economy and Competitiveness (Grant No. PID2019-105898GA-C22) and the Madrid Government (Comunidad de Madrid-Spain) under the Multianual Agreement with Universidad Politécnica de Madrid in the line Excellence Programme for University Professors, in the context of the V PRICIT (Regional Programme of Research and Technological Innovation). J.R.E. also acknowledges funding from the Roger Ekins Research Fellowship of Emmanuel College. This work was performed using resources provided by the Cambridge Tier-2 system operated by the University of Cambridge Research Computing Service (<http://www.hpc.cam.ac.uk>) funded by EPSRC Tier-2 capital Grant No. EP/P020259/1. The authors gratefully acknowledge the Universidad Politécnica de Madrid ([www.upm.es](http://www.upm.es)) for also providing computing resources on Magerit Supercomputer. We thank Pablo Piaggi for sending us the preprint of Ref. 105 prior to publication. E.S. and C.V. acknowledge funding received under Grant No. PID2019-105898GB-C21.

## AUTHOR DECLARATIONS

### Conflict of Interest

The authors have no conflicts to disclose.

### Author Contributions

**Ignacio Sanchez-Burgos:** Formal analysis (lead); Investigation (lead); Methodology (lead); Validation (lead); Visualization (lead); Writing – original draft (lead); Writing – review & editing (lead). **Andres R. Tejedor:** Formal analysis (lead); Investigation (lead); Methodology (lead); Validation (lead); Visualization (lead); Writing – review & editing (equal). **Carlos Vega:** Conceptualization (equal); Methodology (lead); Writing – review & editing (supporting). **Maria M. Conde:** Methodology (equal); Writing – review & editing (supporting). **Eduardo Sanz:** Conceptualization (equal); Methodology (lead); Writing – review & editing (equal). **Jorge Ramirez:** Conceptualization (equal); Formal analysis (lead); Funding acquisition (equal); Investigation (lead); Methodology (equal); Resources (equal); Validation (equal); Visualization (equal); Writing – review & editing (supporting). **Jorge R. Espinosa:** Conceptualization (lead); Funding acquisition (lead); Investigation (equal); Methodology (lead); Project administration (lead); Resources (lead); Supervision (lead); Writing – review & editing (lead).

## DATA AVAILABILITY

The data that support the findings of this study are available within the article.

## REFERENCES

- <sup>1</sup>S. A. Zielke, A. K. Bertram, and G. N. Patey, *J. Phys. Chem. B* **119**, 9049 (2015).
- <sup>2</sup>L. Lupi, A. Hudait, and V. Molinero, *J. Am. Chem. Soc.* **136**, 3156 (2014).
- <sup>3</sup>R. Cabriolu and T. Li, *Phys. Rev. E* **91**, 052402 (2015).
- <sup>4</sup>D. Kashchiev, *Nucleation* (Elsevier, 2000).
- <sup>5</sup>P. G. Debenedetti, *Metastable Liquids* (Princeton University Press, 2021).
- <sup>6</sup>K. F. Kelton, *Solid State Phys.* **45**, 75–177 (1991).
- <sup>7</sup>W. Cantrell and A. Heymsfield, *Bull. Am. Meteorol. Soc.* **86**, 795 (2005).
- <sup>8</sup>P. J. DeMott, A. J. Prenni, X. Liu, S. M. Kreidenweis, M. D. Petters, C. H. Twohy, M. S. Richardson, T. Eidhammer, and D. C. Rogers, *Proc. Natl. Acad. Sci. U. S. A.* **107**, 11217 (2010).
- <sup>9</sup>C. S. Zender and J. T. Kiehl, *J. Geophys. Res.: Atmos.* **99**, 25869, <https://doi.org/10.1029/94jd02090> (1994).
- <sup>10</sup>D. A. Hegg and M. B. Baker, *Rep. Prog. Phys.* **72**, 056801 (2009).
- <sup>11</sup>A. Hudait and V. Molinero, *J. Am. Chem. Soc.* **138**, 8958 (2016).
- <sup>12</sup>B. Kärcher and A. Seifert, *Q. J. R. Meteorol. Soc.* **142**, 1320 (2016).
- <sup>13</sup>L. R. Maki, E. L. Galyan, M.-M. Chang-Chien, and D. R. Caldwell, *Appl. Microbiol.* **28**, 456 (1974).
- <sup>14</sup>H. Kiani and D.-W. Sun, *Trends Food Sci. Technol.* **22**, 407 (2011).
- <sup>15</sup>E. B. Moore and V. Molinero, *Nature* **479**, 506 (2011).
- <sup>16</sup>D. A. Knopf and Y. J. Rigg, *J. Phys. Chem. A* **115**, 762 (2011).
- <sup>17</sup>H. R. Pruppacher, *J. Atmos. Sci.* **52**, 1924 (1995).
- <sup>18</sup>J. Gerrard, *Rocks and Landforms* (Springer Science & Business Media, 2012).
- <sup>19</sup>G. D. Ashton, *River and Lake Ice Engineering* (Water Resources Publication, 1986).
- <sup>20</sup>C. A. Stan, G. F. Schneider, S. S. Shevkopyas, M. Hashimoto, M. Ibanescu, B. J. Wiley, and G. M. Whitesides, *Lab Chip* **9**, 2293 (2009).
- <sup>21</sup>P. Taborek, *Phys. Rev. B* **32**, 5902 (1985).
- <sup>22</sup>P. J. DeMott and D. C. Rogers, *J. Atmos. Sci.* **47**, 1056 (1990).
- <sup>23</sup>P. Stöckel, I. M. Weidinger, H. Baumgärtel, and T. Leisner, *J. Phys. Chem. A* **109**, 2540 (2005).
- <sup>24</sup>B. Krämer, O. Hübner, H. Vortisch, L. Wöste, T. Leisner, M. Schwell, E. Rühl, and H. Baumgärtel, *J. Chem. Phys.* **111**, 6521 (1999).
- <sup>25</sup>D. Duft and T. Leisner, *Atmos. Chem. Phys.* **4**, 1997 (2004).
- <sup>26</sup>H. Laksmono, T. A. McQueen, J. A. Sellberg, N. D. Loh, C. Huang, D. Schlesinger, R. G. Sierra, C. Y. Hampton, D. Nordlund, M. Beye *et al.*, *J. Phys. Chem. Lett.* **6**, 2826 (2015).
- <sup>27</sup>E. Sanz, C. Vega, J. R. Espinosa, R. Caballero-Bernal, J. L. F. Abascal, and C. Valeriani, *J. Am. Chem. Soc.* **135**, 15008 (2013).
- <sup>28</sup>A. J. Amaya and B. E. Wyslouzil, *J. Chem. Phys.* **148**, 084501 (2018).
- <sup>29</sup>A. Manka, H. Pathak, S. Tanimura, J. Wölk, R. Strey, and B. E. Wyslouzil, *Phys. Chem. Chem. Phys.* **14**, 4505 (2012).
- <sup>30</sup>L. S. Bartell and Y. G. Chushak, *Water in Confining Geometries* (Springer, 2003), pp. 399–424.
- <sup>31</sup>D. E. Hagen, R. J. Anderson, and J. L. Kassner, Jr., *J. Atmos. Sci.* **38**, 1236 (1981).
- <sup>32</sup>S. Auer and D. Frenkel, *J. Chem. Phys.* **120**, 3015 (2004).
- <sup>33</sup>L. Filion, M. Hermes, R. Ni, and M. Dijkstra, *J. Chem. Phys.* **133**, 244115 (2010).
- <sup>34</sup>J. R. Espinosa, C. Vega, C. Valeriani, and E. Sanz, *J. Chem. Phys.* **144**, 034501 (2016).
- <sup>35</sup>I. Sanchez-Burgos, E. Sanz, C. Vega, and J. R. Espinosa, *Phys. Chem. Chem. Phys.* **23**, 19611 (2021).
- <sup>36</sup>P. Montero de Hijes, J. R. Espinosa, V. Bianco, E. Sanz, and C. Vega, *J. Phys. Chem. C* **124**, 8795 (2020).
- <sup>37</sup>J. R. Espinosa, C. Vega, C. Valeriani, D. Frenkel, and E. Sanz, *Soft Matter* **15**, 9625 (2019).
- <sup>38</sup>P. Rein ten Wolde, M. J. Ruiz-Montero, and D. Frenkel, *J. Chem. Phys.* **104**, 9932 (1996).
- <sup>39</sup>H. Vehkamäki and I. J. Ford, *J. Chem. Phys.* **112**, 4193 (2000).
- <sup>40</sup>V. G. Baidakov, A. O. Tipseev, K. S. Bobrov, and G. V. Ionov, *J. Chem. Phys.* **132**, 234505 (2010).
- <sup>41</sup>K. K. Tanaka, H. Tanaka, T. Yamamoto, and K. Kawamura, *J. Chem. Phys.* **134**, 204313 (2011).
- <sup>42</sup>P. R. ten Wolde and D. Frenkel, *J. Chem. Phys.* **109**, 9901 (1998).
- <sup>43</sup>P. Rosales-Pelaez, I. Sanchez-Burgos, C. Valeriani, C. Vega, and E. Sanz, *Phys. Rev. E* **101**, 022611 (2020).
- <sup>44</sup>I. Sanchez-Burgos, P. M. de Hijes, P. Rosales-Pelaez, C. Vega, and E. Sanz, *Phys. Rev. E* **102**, 062609 (2020).
- <sup>45</sup>A. O. Tipseev, E. D. Zanotto, and J. P. Rino, *J. Phys. Chem. C* **122**, 28884 (2018).
- <sup>46</sup>N. E. R. Zimmermann, B. Vorselaars, D. Quigley, and B. Peters, *J. Am. Chem. Soc.* **137**, 13352 (2015).
- <sup>47</sup>C. Valeriani, E. Sanz, and D. Frenkel, *J. Chem. Phys.* **122**, 194501 (2005).
- <sup>48</sup>C. P. Lamas, J. R. Espinosa, M. M. Conde, J. Ramírez, P. Montero de Hijes, E. G. Noya, C. Vega, and E. Sanz, *Phys. Chem. Chem. Phys.* **23**, 26843 (2021).
- <sup>49</sup>H. Jiang, A. Haji-Akbari, P. G. Debenedetti, and A. Z. Panagiotopoulos, *J. Chem. Phys.* **148**, 044505 (2018).
- <sup>50</sup>L. Separdar, J. P. Rino, and E. D. Zanotto, *Comput. Mater. Sci.* **187**, 110124 (2021).
- <sup>51</sup>S. C. C. Prado, J. P. Rino, and E. D. Zanotto, *Comput. Mater. Sci.* **161**, 99 (2019).
- <sup>52</sup>A. O. Tipseev and E. D. Zanotto, *Chem. Phys. Lett.* **735**, 136749 (2019).
- <sup>53</sup>D. Yuhara, B. C. Barnes, D. Suh, B. C. Knott, G. T. Beckham, K. Yasuoka, D. T. Wu, and A. K. Sum, *Faraday Discuss.* **179**, 463 (2015).
- <sup>54</sup>P. Yi, C. R. Locker, and G. C. Rutledge, *Macromolecules* **46**, 4723 (2013).
- <sup>55</sup>I. Saika-Voivod, F. Romano, and F. Sciortino, *J. Chem. Phys.* **135**, 124506 (2011).
- <sup>56</sup>T. Li, D. Donadio, G. Russo, and G. Galli, *Phys. Chem. Chem. Phys.* **13**, 19807 (2011).
- <sup>57</sup>A. Haji-Akbari, R. S. DeFever, S. Sarupria, and P. G. Debenedetti, *Phys. Chem. Chem. Phys.* **16**, 25916 (2014).
- <sup>58</sup>J. Russo, F. Romano, and H. Tanaka, *Nat. Mater.* **13**, 733 (2014).
- <sup>59</sup>B. Cheng, C. Dellago, and M. Ceriotti, *Phys. Chem. Chem. Phys.* **20**, 28732 (2018).
- <sup>60</sup>H. Niu, Y. I. Yang, and M. Parrinello, *Phys. Rev. Lett.* **122**, 245501 (2019).
- <sup>61</sup>J. R. Espinosa, C. Navarro, E. Sanz, C. Valeriani, and C. Vega, *J. Chem. Phys.* **145**, 211922 (2016).
- <sup>62</sup>R. J. Allen, P. B. Warren, and P. R. Ten Wolde, *Phys. Rev. Lett.* **94**, 018104 (2005).
- <sup>63</sup>P. G. Bolhuis, D. Chandler, C. Dellago, and P. L. Geissler, *Annu. Rev. Phys. Chem.* **53**, 291 (2002).
- <sup>64</sup>A. Barducci, G. Bussi, and M. Parrinello, *Phys. Rev. Lett.* **100**, 020603 (2008).
- <sup>65</sup>A. Laio and F. L. Gervasio, *Rep. Prog. Phys.* **71**, 126601 (2008).
- <sup>66</sup>G. M. Torrie and J. P. Valleau, *Chem. Phys. Lett.* **28**, 578 (1974).
- <sup>67</sup>A. Reinhardt, J. P. K. Doye, E. G. Noya, and C. Vega, *J. Chem. Phys.* **137**, 194504 (2012).
- <sup>68</sup>A. Haji-Akbari and P. G. Debenedetti, *Proc. Natl. Acad. Sci. U. S. A.* **112**, 10582 (2015).
- <sup>69</sup>M. Chopra, A. S. Reddy, N. Abbott, and J. De Pablo, *J. Chem. Phys.* **129**, 135102 (2008).
- <sup>70</sup>F. A. Escobedo, E. E. Borrero, and J. C. Araque, *J. Phys.: Condens. Matter* **21**, 333101 (2009).
- <sup>71</sup>M. Volmer and A. Weber, *Z. Phys. Chem.* **119**, 277 (1926).
- <sup>72</sup>R. Becker and W. Döring, *Ann. Phys.* **416**, 719 (1935).
- <sup>73</sup>J. Merikanto, E. Zapadinsky, A. Lauri, and H. Vehkamäki, *Phys. Rev. Lett.* **98**, 145702 (2007).
- <sup>74</sup>S. Ryu and W. Cai, *Phys. Rev. E* **81**, 030601 (2010).
- <sup>75</sup>F. Leoni and J. Russo, *Phys. Rev. X* **11**, 031006 (2021).
- <sup>76</sup>N. E. R. Zimmermann, B. Vorselaars, J. R. Espinosa, D. Quigley, W. R. Smith, E. Sanz, C. Vega, and B. Peters, *J. Chem. Phys.* **148**, 222838 (2018).
- <sup>77</sup>J. R. Espinosa, P. Sampedro, C. Valeriani, C. Vega, and E. Sanz, *Faraday Discuss.* **195**, 569 (2016).
- <sup>78</sup>V. Molinero and E. B. Moore, *J. Phys. Chem. B* **113**, 4008 (2009).

- <sup>79</sup>J. L. F. Abascal, E. Sanz, R. García Fernández, and C. Vega, *J. Chem. Phys.* **122**, 234511 (2005).
- <sup>80</sup>J. R. Espinosa, C. Vega, and E. Sanz, *J. Phys. Chem. C* **120**, 8068 (2016).
- <sup>81</sup>M. De Marzio, G. Camisasca, M. Rovere, and P. Gallo, *Front. Phys.* **13**, 136103 (2018).
- <sup>82</sup>P. Gallo, J. Bachler, L. E. Bove, R. Böhmer, G. Camisasca, L. E. Coronas, H. R. Corti, I. de Almeida Ribeiro, M. de Koning, G. Franzese *et al.*, *Eur. Phys. J. E* **44**, 143 (2021).
- <sup>83</sup>P. G. Debenedetti, F. Sciortino, and G. H. Zerze, *Science* **369**, 289 (2020).
- <sup>84</sup>J. R. Espinosa, C. Vega, and E. Sanz, *J. Phys. Chem. C* **122**, 22892 (2018).
- <sup>85</sup>J. Algaba, E. Acuña, J. M. Míguez, B. Mendiboure, I. M. Zerón, and F. J. Blas, *J. Colloid Interface Sci.* **623**, 354 (2022).
- <sup>86</sup>J. R. Espinosa, C. Vega, and E. Sanz, *J. Chem. Phys.* **141**, 134709 (2014).
- <sup>87</sup>S. Plimpton, *J. Comput. Phys.* **117**, 1 (1995).
- <sup>88</sup>S. Nosé, *J. Chem. Phys.* **81**, 511 (1984).
- <sup>89</sup>W. G. Hoover, *Phys. Rev. A* **31**, 1695 (1985).
- <sup>90</sup>W. G. Hoover, *Phys. Rev. A* **34**, 2499 (1986).
- <sup>91</sup>A. Haji-Akbari, *J. Chem. Phys.* **149**, 072303 (2018).
- <sup>92</sup>R. W. Hockney and J. W. Eastwood, *Computer Simulation Using Particles* (CRC Press, 2021).
- <sup>93</sup>D. Atherton, A. Michaelides, and S. J. Cox, *J. Chem. Phys.* **156**, 164501 (2022).
- <sup>94</sup>J.-P. Ryckaert, G. Ciccotti, and H. J. C. Berendsen, *J. Comput. Phys.* **23**, 327 (1977).
- <sup>95</sup>A. Stukowski, *Modell. Simul. Mater. Sci. Eng.* **18**, 015012 (2009).
- <sup>96</sup>S. Luo, J. Wang, and Z. Li, *J. Phys. Chem. B* **124**, 3701 (2020).
- <sup>97</sup>W. Lechner and C. Dellago, *J. Chem. Phys.* **129**, 114707 (2008).
- <sup>98</sup>J. R. Espinosa, A. Zaragoza, P. Rosales-Pelaez, C. Navarro, C. Valeriani, C. Vega, and E. Sanz, *Phys. Rev. Lett.* **117**, 135702 (2016).
- <sup>99</sup>J. Benet, P. Llombart, E. Sanz, and L. G. MacDowell, *Mol. Phys.* **117**, 2846 (2019).
- <sup>100</sup>D. N. Sibley, P. Llombart, E. G. Noya, A. J. Archer, and L. G. MacDowell, *Nat. Commun.* **12**, 239 (2021).
- <sup>101</sup>V. Bianco, P. M. de Hijos, C. P. Lamas, E. Sanz, and C. Vega, *Phys. Rev. Lett.* **126**, 015704 (2021).
- <sup>102</sup>C. Vega, J. L. F. Abascal, M. M. Conde, and J. L. Aragones, *Faraday Discuss.* **141**, 251 (2009).
- <sup>103</sup>I. Sanchez-Burgos, A. Garaizar, C. Vega, E. Sanz, and J. R. Espinosa, *Soft Matter* **17**, 489 (2021).
- <sup>104</sup>A. Hudait, S. Qiu, L. Lupi, and V. Molinero, *Phys. Chem. Chem. Phys.* **18**, 9544 (2016).
- <sup>105</sup>P. M. Piaggi, J. Weis, A. Z. Panagiotopoulos, P. G. Debenedetti, and R. Car, [arXiv:2203.01376](https://arxiv.org/abs/2203.01376) (2022).
- <sup>106</sup>L. Vrbka and P. Jungwirth, *J. Phys. Chem. B* **110**, 18126 (2006).
- <sup>107</sup>E. Pluhařová, L. Vrbka, and P. Jungwirth, *J. Phys. Chem. C* **114**, 7831 (2010).